

INVITED REVIEWS

Detection and Assessment of Congenital Heart Disease with Magnetic Resonance Techniques

Christoph A. Nienaber, Tim C. Rehders, and Sohrab Fratz

Department of Cardiology, University Hospital Eppendorf, Hamburg, Germany

INTRODUCTION

Although chest radiography remains the initial imaging modality in the work-up of congenital heart disease (CHD), the cardiovascular community is often overburdened and at a loss to establish the correct diagnosis on the basis of plane chest films (Fig. 1). Thus, with echocardiography in their hands, pediatric cardiologists have become the principle investigators of patients with CHD. Moreover, approximately half of CHD is due to isolated septal abnormalities easily emendable to echocardiography with Doppler interrogation. However, complex lesions, especially those involving the central pulmonary vasculature and right-sided heart lesions, are difficult to assess even with transesophageal echocardiography (1–3) and are dependent on operator competence. Although the technique allows multiplanar imaging, compliance of the patient, body habit limitations, previous surgery, and pulmonary abnormalities may inhibit visualization of complex structures. In more difficult and complex cases of CHD, catheter angiography has been the traditional imaging modality of choice. However, angiography is invasive, traumatic to femoral and subclavian vessels of small children, and involves contrast dye of potential nephrotoxicity. Moreover, in CHD, repeated and follow-up diagnostics are often required to delineate the entire extent of the anomaly and follow its course over time;

the latter clearly speaks for a noninvasive nontoxic modality such as magnetic resonance imaging (MRI).

Spin-echo (SE) MRI is a superb noninvasive non-ionizing imaging modality that when gated to the patient's heart and respiratory rate or as a breathhold technique provides excellent imaging of the pathoanatomy of CHD. In addition, MRI is excellent at delineating the anatomy of the great vessels (4,5). Although, still evolving, this technique combines the major strength of the more traditional imaging modalities and offers also functional information on the underlying anatomic anomaly (6). The large field of view (FOV) in any desired plane allows simultaneous visualization of all cardiac chambers, the great vessels, the bronchial tree, and the abdomen (7). These factors, coupled with improved spatial resolution, make MRI attractive to surgeons, who are accustomed to angiographic evaluation. On gradient-recalled echo (GRE), MR flowing blood, both arterial and venous, may be visualized without contrast agents (8), or, even better, MR angiography (MRA) with gadolinium shows the entire vasculature structure in three-dimensional display. Thus, MRI can be used as an adjunct to chest x-ray and echocardiography for any of the reasons already mentioned; as a primary imaging modality, MRI is useful in more complex cases and in the evaluation of the great vessels.

The purpose of this article is to review the various

Received September 4, 1998; Accepted December 4, 1998
Address reprint requests to C. A. Nienaber.

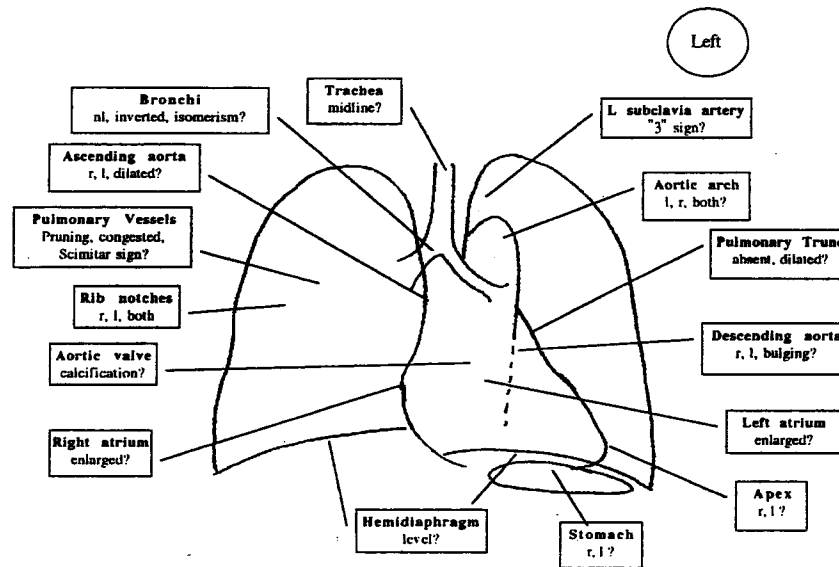


Figure 1. Features of congenital heart disease on conventional chest film or coronal MRI. (Adapted from Kilner P. Imaging of adults with congenital heart disease. In: Lima J, ed. *Diagnostic Imaging in Clinical Cardiology*. Baltimore: Martin Dunitz; 1998.)

options of MRI relevant to the evaluation of CHD, including recent developments in MRI technology likely to increase the utility of MR in cardiology. The article will also provide an overview of fundamental cardiovascular embryology and will define areas in which MRI has proven to be most useful in the diagnostic work-up of patients with CHD and at least equally sensitive and specific as compared with transesophageal echocardiography and angiography in the entire spectrum of CHD (5,9).

TECHNICAL OPTIONS OF MRI

SE MRI

Multislice SE MRI with triggering of the image acquisition by the electrocardiogram (ECG) is the most commonly applied technique to define the morphology of the heart and great vessels. Images are routinely obtained in the transverse plane, with additional imaging planes tailored to the cardiovascular structures under investigation (Fig. 2). The SE images are acquired with relatively short repetition times (TR), dependent on the heart rate when ECG-triggering is used, and short echo times (TE), usually 20–30 msec long and with two to four averages to optimize the signal-to-noise ratio. This imaging sequence is especially well suited for defining anatomic detail but allows no assessment of dynamic cardiac events because moving blood does not produce a signal and provides

good contrast with the surrounding structures (e.g., myocardium or vessel wall) (10). When a stack of SE sections is required, each section corresponds to a different cardiac phase, without functional information of dynamic processes throughout a cardiac cycle.

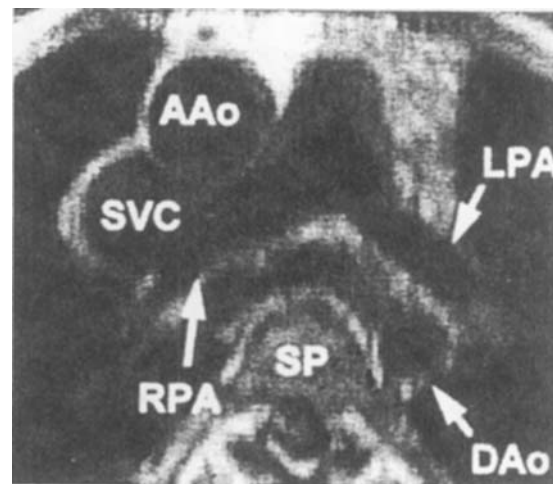


Figure 2. Patient after Hemi-Fontan operation to shunt venous blood into pulmonary circulation. The coronal SE MRI demonstrates the anatomic situs better than any alternative imaging modality and allows exact quantitative assessment of pulmonary artery diameter. AAO, ascending aorta; DAO, descending aorta; LPA, left pulmonary artery; RPA, right pulmonary artery; SVC, superior vena cava; SP, spine.

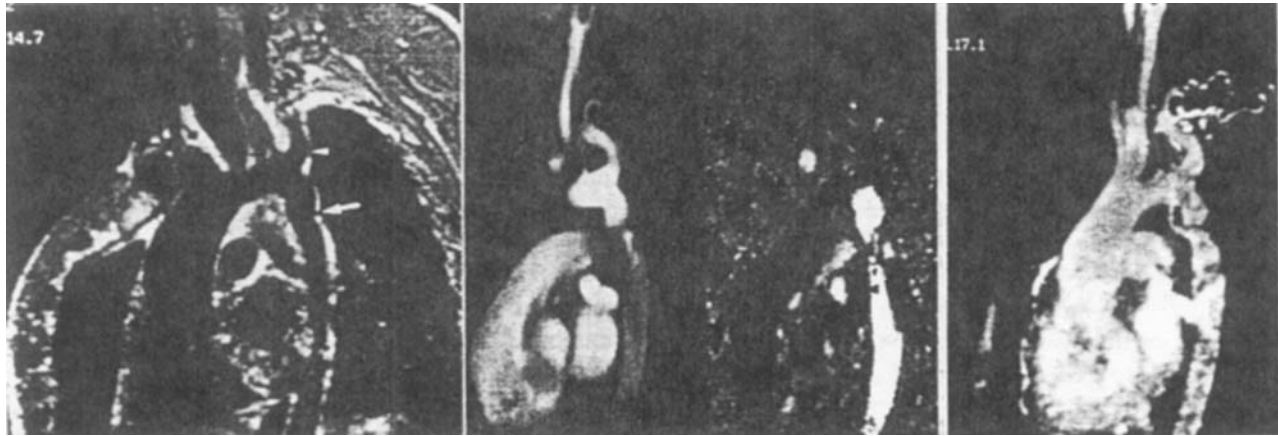


Figure 3. Left: Anatomic SE MRI showing the exact site of coarctation. Middle: cine MRI (or GRE image) revealing the functional severity of the aortic isthmus stenosis with evidence of turbulent flow shown by the characteristic signal void, both on cine MRI and phase mapping. Right: MRA after intravenous injection of gadolinium-DTPA nicely delineating the stenotic site, the development of the collateral circulation, and the adjacent vasculature.

GRE MRI

In contrast with SE techniques, GRE MRI provides less soft tissue detail but dynamic information on flow and cardiac function (11). GRE images display flowing blood as a bright signal intensity, whereas SE images show flowing blood generally as a dark signal or a signal void (12). On GRE cine displays, disturbances of normal flow are shown as low-signal turbulent jet effects. GRE images are acquired with high temporal resolution throughout the cardiac cycle of 8–16 frames/sec by using short TR, short TE, and small flip angles (10). This technique is ideally suited to assess functional information on aortic coarctation (Fig. 3, A and B). However, the image acquisition is not real time but requires, for example, 128 heartbeats for images with 128 phase-encoding steps. The images can be displayed in a cine mode at the above frame rate to reveal the dynamics of flow and other motion effects in a pseudo-real-time format. Artifacts inherent to GRE techniques pose a problem when one images structures such as metallic implants or anatomic structures adjacent to the lung parenchyma because of susceptibility effects.

Ultrafast MRI

Recently, ultrafast gradient MRI and real-time echoplanar techniques have been introduced into clinical practice (13,14). Fast-imaging methods reduce image degradation from physiologic motion effects such as respiration and cardiac rotation during contraction, allowing

improved evaluation of cardiovascular function. Ultrafast MRI allows image acquisition during a breathhold within one heartbeat's interval. These rapid gradient echo sequences operate with very short TR values, resulting in suboptimal image contrast. A prepulse is commonly applied to suppress vascular signal and provide T1-weighted contrast in the final image. To restore T1 and T2 image contrast, preparatory pulses are incorporated in the imaging sequence in the time interval before data collection starts. For example, this technique is applied to assess first-pass myocardial perfusion with the aid of various intravascular contrast agents used as perfusion markers (Fig. 3C) (15).

Echoplanar imaging (EPI) provides snapshot or multishot imaging with very short acquisition times of 20–100 msec per image, allowing real-time imaging of cardiac function and flow with acquisition rates of up to 50 images per second (14). In EPI, multiple segments of the image data are acquired from a single SE or GRE. The acquisition of an entire image after a single radiofrequency excitation is performed, for example, for a 128 phase-encoded image with 128 oscillations of the readout gradient. The readout gradient oscillates rapidly from positive to negative amplitude to form a train of GRE that form around the envelope of the SE induced by a single excitation. Each echo is differently phase encoded by phase-encoded "blips" on the phase axis. EPI technology poses special demands on the gradient system and radiofrequency receiver of the MR scanner. With further technical advances, EPI may become clinically applicable for multislice imaging of the entire heart within a

single heartbeat. EPI images of the heart can be acquired without the need for ECG triggering in a free-run mode and displayed in a cine format to demonstrate dynamic processes such as a valve function, flow, and perfusion (16,17).

Fast SE or turbo-SE (TSE) MRI allows the acquisition of high-quality T2-weighted MR images with substantial reduction in imaging time, compared with conventional T2-weighted MR sequences (18). T2-weighted MRI is valuable in obtaining better characterization of the composition of tissue components, such as intramural hematoma of the aorta (19). However, conventional T2-weighted approaches suffer from several artifacts due to motion during relatively long acquisition times. This problem may be overcome with the use of TSE acquisition. Reduced imaging time with ECG-triggered TSE imaging is achievable because of acquisition of multiple phase-encoding steps for each excitation in combination with the multislice mode. TSE imaging obviates the use of time-consuming conventional T2-weighted preparations while maintaining high-quality T2 information for improved tissue characterization and improved definition of cardiac and mediastinal abnormalities.

Flow Mapping and MRA

MRA is based on a number of GRE MR techniques that allow the visualization of flowing blood noninvasively. These techniques are categorized as time-of-flight or phase-contrast methods, depending on the principle for visualization of flowing blood (20). In the time-of-flight method, the difference between the signal obtained from flowing blood and that from stationary tissue is due to the continuous wash-in of unsaturated blood and wash-out of saturated blood within an imaging section. This phenomenon of flow-related enhancement results in bright vessels on a relatively dark background (21). In the phase-contrast method, the difference in signal intensity between flowing and stationary structures is based on velocity-induced phase shifts of moving spins in the presence of a magnetic field gradient (22,23). In contrast to most MRI techniques, images are reconstructed from the phase of the MR signal rather than from the amplitude. This approach allows the extraction of quantitative flow information, because the phase shift of flowing blood is proportional to its velocity. So far, MR velocity mapping provides accurate measurement of flow velocity and flow volume in medium and large vascular structures. MR velocity mapping has been validated as an accurate technique both in vitro and in vivo (24). This phase-contrast-

based method is gaining widespread acceptance as a valuable technique for measuring flow in the aorta, pulmonary arteries, superior caval vein, pulmonary veins, and, possibly in the future, coronary circulation, flow across cardiac valves, and flow in other vascular structures throughout the body (25–27). MR velocity mapping correlates well with oximetry and with MR measurements based on ventricular volumetry for calculation of shunt size in patients with CHD, including atrial (ASD) and ventricular septal defects (VSD), persistent ductus arteriosus (PDA), truncus arteriosus, and coronary-to-pulmonary artery fistulas (27a).

Three-Dimensional Contrast-Enhanced MRA

Especially complex CHD may prove extremely suitable for MRI and three-dimensional (3-D) MRA after bolus injection of gadolinium-diethylenetriaminopentacetic acid (DTPA) via a venous access (28,29). Based on the administration of gadolinium during data acquisition, the technique exploits the contrast-induced T1-shortening effects and avoids saturation problems with slow flow or turbulence-induced signal voids. With the use of ultrafast gradients, acquisition has to be performed at breathhold of 15–25 sec. A fast spoiled gradient 3-D sequence with and without intravenous contrast is the basis for creating maximum intensity projections; TE and TR may be set at 1.9 and 4.0 msec, respectively. With a FOV between 390 and 450 mm, a conventional 512×512 matrix provides an in-plane resolution of 1.1×1.6 mm. Slice thickness may vary from 2 to 4 mm, and the flip angle of 30 degrees is usually used. High-quality imaging of 64 interpolated contiguous slices using $1/2$ K-space data acquisition in phase-encoding direction usually takes about 15–25 sec, and acquisition is performed with a 1.5-T MR equipped with an ultrafast gradient system; a dedicated body array coil is needed for signal transmission and reception. Optimal image quality is ensured by individual bolus tracking before infusion of 0.25 mmol/kg body weight of gadolinium over 10–30 sec (half the acquisition time). With subvolume multiplanar reconstruction, the intra- and extracardiac structures (Fig. 3C), the exact site of a malformation, or pathologic intracardiac connection is identified and visualized in 3-D fashion (Fig. 4). The morphometric evaluation of MR images and angiograms may be extremely helpful to determine even the most complex abnormality, to describe the anatomic situs, to plan a corrective operation, and to assess the postsurgical result (Fig. 5).

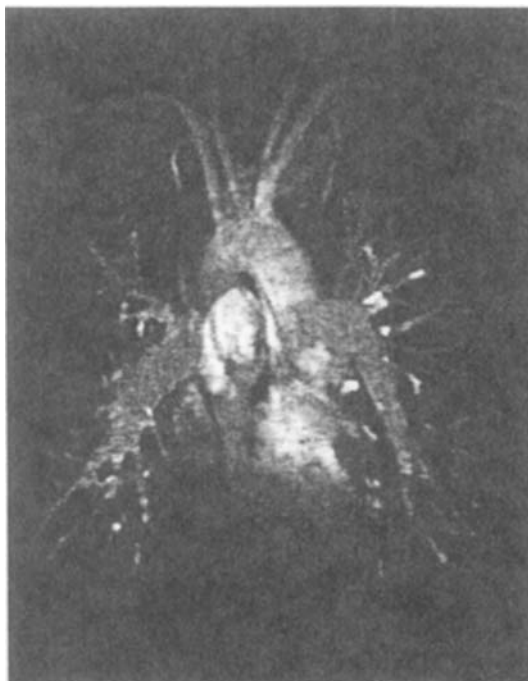


Figure 4. MRA after gadolinium-DTPA showing the lumino-gram of a patient with double-inlet left ventricle (or functionally a univentricular heart). The aorta and pulmonary vasculature originate from the “single chamber”; no septum is appreciated.



Figure 5. MRA of a patient after previous modified Rastelli shunt operation in TGA; the MRA clarifies the fact that the shunts are open and well perfused and confirms a good result 8 yr postsurgery.

CARDIAC EMBRYOLOGY

The standpoint of an embryologist greatly helps to understand the formation and septation of the atrial and systemic veins, the ventricles, and the great arteries and thus complex congenital cardiac anomalies (30). The formation of two single endocardial tubes begins at day 21 after fertilization with sequential primordial heart chambers such as the sinus venosus, the primitive atrium, the primitive ventricle, bulbus, conus, and truncus arteriosus that continues into the aortic sac. The primitive heart tubes join centrally to form a bulboventricular loop (31–33). Within the following 10 days, the partitioning of the primitive heart and the transformation from a single- to a four-chambered heart is performed. Blood enters the heart through paired venous structures, passes through a differentiated endocardial tube, and leaves through paired arterial structures, the conotruncal apparatus. With septation of the various structures, a four-chambered heart and two great arteries are created (31–33). Under normal conditions the left-sided venous structures and the left sinus venosus regress. The right sinus venosus becomes incorporated into the right atrium, constituting the entire smooth-walled portion of the adult right atrium. The atrial appendage is the only remnant of the embryonic right atrium. The left atrial appendage is the remnant of the embryonic left atrium, whereas the left atrium consists of a fusion with a common pulmonary vein. The inferior vena cava (IVC) drains into the right-sided right atrium in the normal or situs solitus situation (31–33).

The septation of the atria is stimulated by the truncus arteriosus to form a septum primum that never completely divides the common atrium. A persistent opening between the two atria is known as the ostium primum. The ostium primum lies just above the communication of the atria with the left ventricle (e.g., the atrioventricular [AV] canal), whereas the septum and ostium secundum is situated above. After birth, the foramen ovale situated in this region closes and forms the thin-walled fossa ovalis; in 20% of the population, the foramen ovale remains probe patent (31–33). At day 42 the communication between the atria and ventricles, the AV canal, is septated by the endocardial cushions. A set of medial and lateral cushions divides the AV canal into a right and a left AV orifice and helps to form a component of the tricuspid valve and the anterior leaflet of the mitral valve and the chordae tendineae and papillary muscles. The remaining AV valve leaflets are not derived from the atria but from their respective ventricles. Therefore, in cases of ventricular inversion (e.g., in congenitally corrected transposition of the great arteries [cc-TGA]), each AV

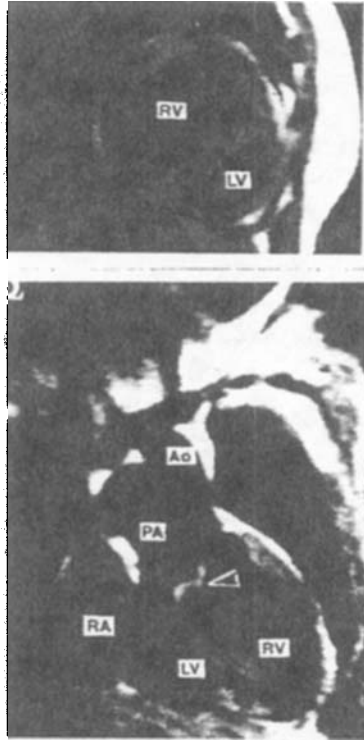


Figure 6. Corrected TGA in double oblique and coronal orientation. The SE MRI reveals transposition with the aorta (Ao) originating from the anatomic right ventricle (RV) and the left ventricle (LV) connected to the right atrium (RA) and pulmonary artery (PA).

valve stays with its ventricle (Fig. 6). With expansion of both the right and left ventricle, the trabeculated muscular interventricular septum is formed. A large trabecula on the right, the septal band, runs longitudinally to the apex. Another prominent trabecula, the moderator band, connects with the anterior papillary muscle (31–33). The membranous septum constitutes the superior part of the septum that extends over the tricuspid valve. Thus, a defect in the supra-ventricular portion of the membranous septum infers a left ventricular-to-right arterial shunt.

Septations of the conus cordis and the truncus arteriosus are intimately related and eventually form the ascending aorta, main pulmonary artery, infundibulum, or outflow tract of the right ventricle, aortic annulus, semilunar valves, and the AV canal and the muscular interventricular septum. Pairs of truncal and conal swellings, similar to the endocardial cushions, appear in the truncus arteriosus and the conus cordis. The fusion of the dextro-superior and sinistroinferior truncal swellings and the dextrodorsal and sinistroventral conal swellings deter-

mine the relation between aorta and main pulmonary arteries. The truncal swellings divide the truncus arteriosus into an aortic channel (proximal ascending aorta) and a pulmonary channel (pulmonary trunk). Because the conotruncal apparatus is intimately involved in the formation of the great arteries, interventricular septum, and endocardial cushions, it appears obvious for an anomaly of the conotruncus to consist of several components (31–33). The septation of the outflow tract is the final morphologic change in the developing heart; meanwhile, aortic and pulmonic valves stem from small tubercles on the truncal swellings and from a tubercle along the free wall of each artery. The leaflets and sinuses of Valsalva form by a process of excavation of the tubercles simultaneously with the final septation of the conotruncal apparatus.

Formation of the aortic arch and its branches is a complex process involving the development of six pairs of aortic arches. The first and second arch basically disappear, with only a part of the first persisting as a portion of the maxillary artery. All that remains of the second arch is the stapedial artery. The fifth aortic arch in mammals is rudimentary. The aortic arch of the adult is formed by the left third arch and is connected with the ductus arteriosus that is a part of the distal sixth aortic arch. Normally, this structure obliterates after birth and is converted to the ligamentum arteriosum. In the embryo, both sixth arches are also continuous with the pulmonary trunk. The right fourth aortic arch persists as part of the proximal subclavian artery.

SYSTEMATIC ANALYSIS OF THE CARDIOVASCULAR ANATOMY

Determination of Situs

Atrial situs solitus is the normal situation with the morphologic right atrium on the right side and the morphologic left atrium on the left side of the body. The atrial situs inversus is the mirror image of the normal situation. In the normal situs solitus, the short main bronchus, the liver, and the IVC are right-sided structures, whereas the long main bronchus, the stomach, the spleen, and the abdominal aorta are left-sided structures (34–36). The morphology of the main bronchi is well visualized on coronal and transversal SE MR images and is a reliable indicator of the atrial situs but can already easily be determined with chest-x-ray (Fig. 1). Moreover, the right pulmonary artery is ventral to a relatively short right main bronchus, whereas the left pulmonary artery crosses over the left main bronchus.

Situs ambiguus is diagnosed when symmetry of the main bronchi and pulmonary arteries is present, for example, as left-sided (or polysplenia syndrome) or right-sided isomerism (or asplenia syndrome). *Situs ambiguus* is usually associated with complex malformations such as a large symmetric liver, absence of the spleen, and location of the IVC and abdominal aorta on the same side of the spine, all in conjunction with complex cardiac abnormalities. In polysplenia syndrome the presence of bilateral long main bronchi, multiple spleens, and interruption of the hepatic segment of the IVC with azygos or hemiazygos vein continuation are characteristic.

In *situs inversus* the morphologic right atrium with systemic venous drainage is located on the left side, whereas the morphologic left atrium with pulmonary venous drainage is located on the right side. The pulmonary veins can be defined with great accuracy by MRI techniques (37). The configuration of the atrial appendages may also be used to distinguish the morphology of the atria by MRI. The morphologic right atrium is characterized by an appendage with a triangular configuration and wide base of implantation into the atrial chamber. The morphologic left atrium has a tubular appendage with a narrow ostium to the main chamber. In most patients, the atrium connected to the IVC is the morphologic right atrium.

Morphology of the Ventricles

The anatomic location of a ventricular compartment or the wall thickness cannot be used to determine the morphology of the situs, because the ventricular position may be reversed in complex cardiac malformations and the wall thickness depends primarily on loading conditions (38). However, the morphologic right and left ventricles can be distinguished in most patients by close analysis of the anatomic characteristics of the ventricles on MR images. Transverse SE MR images at a midventricular level usually reveal the presence of the moderator band as a landmark for the morphologic right ventricle with a trabecular pattern, whereas the inner left ventricular lining is smooth. Furthermore, the septal attachment of the AV valve of the morphologic right ventricle (the tricuspid valve) is caudal and closer to the cardiac apex than of the morphologic left ventricle.

In addition, the presence of a muscular infundibulum is a reliable anatomic marker for characterizing a morphologic right ventricle, even when the other landmarks are difficult to identify (39). Thus MRI using simple SE images is well suited for analyzing complex ventricular abnormalities (40,41). In case of a single ventricle, one

ventricular compartment receives blood through both AV valves and the assignment of the ventricular morphology is dependent on presence or absence of an infundibulum. Without a reliable description of morphology (very rare with MRI), the single ventricle is diagnosed as indeterminate. After evaluation of atrial situs and ventricular morphology, the AV connections are defined.

Ventriculoarterial Connections

The aorta and pulmonary artery are defined by their branching pattern as optimally visualized on transverse SE MR images at the base of the heart; TGA and other large vessel abnormalities are clearly depicted with the use of multiple transverse imaging planes. cc-TGA, for instance, is a congenital cardiac malformation defined by both discordant AV and ventriculoarterial connections. The morphologically right atrium communicates with the morphologically left ventricle through the mitral valve orifice with the pulmonary artery originating from this ventricle. The morphologically left atrium communicates with the morphologically right ventricle through the tricuspid valve. The ascending aorta rises from the infundibulum of the right ventricle and is located to the left and anterior to the main pulmonary artery in *situs solitus*. The terms “congenitally corrected transposition,” “l-transposition,” and “ventricular inversion” are interchangeable (42). Figure 7 explains the relationship of the

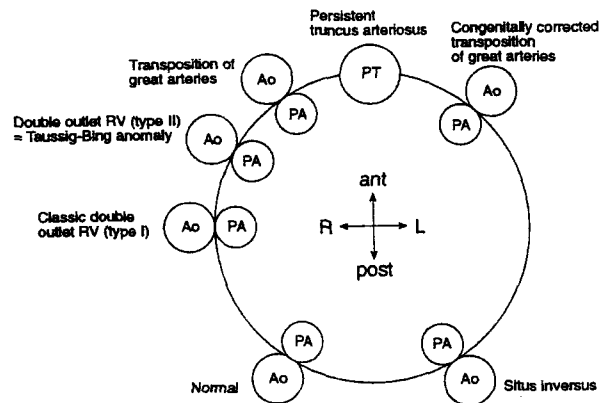


Figure 7. Schema of the relationship between the great arteries in various malformation syndromes in transaxial orientation. (Modified from Ref. 43.) During embryologic development, the primitive truncus is an anterior midline structure. Conotruncal abnormalities are the result of abnormal orientation of the primitive truncus. Ao, aorta; ant, anterior; L, left; PA, pulmonary artery; post, posterior; PT, primitive truncus; R, right; RV, right ventricle.

great vessels in the principal forms of ventriculoarterial connections (43). Besides the advantages for segmental anatomic analysis, MRI is well suited to diagnose vascular rings and other aortic arch anomalies (Fig. 3C) or pulmonary artery malformations (44–46).

Conotruncal Anomalies

Septation anomalies of the conotruncal apparatus in the outflow tracts and at the level of the great arteries are an ideal target for MRI (2,47–49). When septation of the conus cordis and truncus arteriosus fails to develop appropriately, a persistent truncus arteriosus may develop. If septation occurs without the normal spiraling, the result is TGA (Fig. 8). Finally, with asymmetric septation and normal spiraling, the resultant anomaly is tetralogy of Fallot (Fig. 9). Of these three anomalies, MRI is most helpful in evaluation of tetralogy of Fallot. In this anomaly, it is difficult to assess the pulmonary arteries with angiography and echocardiography. Because of its large FOV, multiplanar imaging, and nonreliance on administration of contrast dye, MRI is well suited to display all components of the tetralogy. Moreover, MRI facilitates the identification of the pulmonary arteries, the assessment of their caliber size, and location of collateral vessels (Fig. 9). Furthermore, flow-sensitive MR techniques assess the patency of the ductus arteriosus, the presence



Figure 8. Transverse SE MR image of a patient with TGA. The aorta (A) is situated to the right of and anterior to the main pulmonary artery (P) as schematically shown in Fig. 7. (From Link KM and Lesko NM. Congenital heart disease. In: Edelman RR and Zeatkin MB, eds. *Clinical Magnetic Resonance Imaging*. Philadelphia: WB Saunders; 1996:1698, with permission.)

of bronchial arteries, or major aorticopulmonary collateral arteries arising from the descending aorta in cases of pulmonary atresia. The transaxial views are excellent for evaluating the proximal right and left main pulmonary arteries (2). Imaging perpendicular to the arteries allows precise measurement of vessel diameter. The degree of infundibular stenosis can also be assessed with the transaxial and coronal planes. This determination is useful in assessing the results of infundibulectomy. The severity of pulmonic stenosis, infundibular or valvular, can be assessed using phase-mapping techniques in a plane perpendicular to the pulmonary artery and usually distal to the stenotic lesion. TGA refers to the reversal of the anterior-posterior relationship of the aorta and pulmonary arteries (Fig. 7).

Septation Anomalies

Although MRI can readily establish the diagnosis of a VSD (50,51), ASD (52), or PDA (53), such common septation defects are in general adequately evaluated with echocardiography and color Doppler interrogation. Therefore, MRI is rarely required in their diagnostic workup. If MRI is needed, the short axis view is the most useful orientation for studying ASDs. This “double-oblique” view is oriented perpendicular to the interatrial septum. It is used instead of the standard transaxial view because the atrial septum is quite thin, especially in the area of the fossa ovalis and likely to be misdiagnosed as an ASD on transversal views. Alternatively, cine MRI (or GRE sequences) may demonstrate a black signal void across any, even small, VSDs. Most VSDs are already clearly depicted by standard transaxial imaging. On occasion, a horizontal long-axis view is required to visualize small supravalvular membranous VSDs. This view is usually required when trying to establish the diagnosis of a septal aneurysm. Phase-contrast MRI is useful when there is doubt regarding the diagnosis and as for calculating shunt volumes (54,55). The PDA is difficult to identify on transaxial images. Better visualization can be achieved on a coronal or left anterior oblique (LAO) scan through the aorta, which is best studied using thin-section slices and a dedicated coil. Cine MRI or contrast-enhanced MRA may also be required to establish this diagnosis.

Dextrocardia

Dextrocardia comprises all abnormalities with the heart located predominantly in the right hemithorax. The correct diagnosis can easily be reached by application of

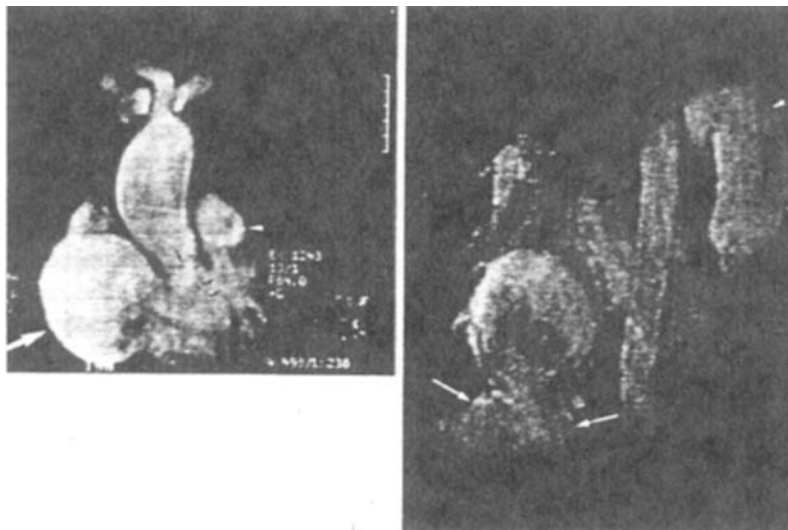


Figure 9. Gadolinium-DTPA-enhanced MRA of a patient with tetralogy of Fallot. Left: MRA showing the ventricular septal defect, overriding aorta, and pulmonary stenosis. Right: Targeted maximum intensity, projection shows dilatation of the left pulmonary artery dilated hepatic veins.

MRI and using three simple rules: the type of aorta determines the loop, the side of the IVC or the bronchi determine the situs (30,56), and in transposition the aorta arises from the right ventricle. The large FOV and sequential multiplanar imaging make MRI much more conducive than echocardiography, conventional angiography, and computed tomography.

There are six types of dextrocardia (Fig. 7) (57) to be distinguished by using coronal and transaxial ECG-gated SE MRI: dextroposition, arrest of the d-bulboventricular loop, situs inversus totalis, cc-TGA, right atrial isomerism, and left atrial isomerism. Examples are shown in Figs. 6, 8, and 10. With the first step (i.e., the determination of the loop type), the presence of an l-bulboventricular loop and thus of either situs inversus totalis or cc-TGA is made. The next step is to determine the situs by evaluating the position of the IVC or the bronchi that identify the right atrium (Fig. 10). Dextroposition is usually associated with a d-bulboventricular loop and situs solitus (the normal situation), but it can also be associated with a simple defect, such as an ASD or a congenital anomaly of the aorta. Associated skeletal abnormalities or pulmonary hypoplasia are best detected in coronal views. Transaxial MR images are better to show the interventricular septum that deviates from its normal 30- to 45-degree orientation relative to the patient's back.

Conversely, *situs inversus totalis* is a mirror image of the normal situation of situs solitus and a d-bulboventri-

cular loop with a 3–5% incidence of congenital abnormalities. Situs inversus is evidenced by a left-sided IVC and therefore left-sided right atrium, and an l-bulboventricular loop is determined by the evidence of an l-aorta. Although the heart is in the right hemithorax, the left ventricle continues to be posterior to the right ventricle and the aorta remains posterior to the pulmonary artery. In TGA a situs solitus and an l-aorta are observed; the aorta is to the left and anterior to the pulmonary artery, arising from the right ventricle. Transaxial and coronal SE MR images delineate the anatomy, and dynamic MRI techniques are used to assess the severity of the associated pulmonary stenosis (44,58). In addition to identifying the components of cc-TGA, it is important to assess the size of the pulmonary arteries and their collateral flow. These patients often require a shunt operation for flow to the pulmonary circulation. Evaluation of the pulmonary arteries is best accomplished using transaxial SE MRI (Fig. 2).

In cases of *atrial isomerism* there are either two right atria or two left atria. Isomerism is often seen by the abdominal relationship of the IVC and the aorta and by polysplenia or asplenia. Typically, the IVC and aorta are on the same side of the spine (juxtaposed) in cases of right atrial isomerism, and there is IVC interruption in 85% of cases of left isomerism. Moreover, the bronchial anatomy may be helpful; if both bronchi are similar in length and angulation, there is atrial isomerism (Fig. 1).



Figure 10. Sagittal SE MR image of a patient with atrial situs inversus. The IVC enters the dorsally located morphologic right atrium. (From de Roos A, Rebergen SA and van der Wall EE. Congenital heart disease assessed with magnetic resonance techniques. In: Skorton DJ, Schelbert HR, Wolff GL and Brundage BH, eds. *Cardiac Imaging*. Philadelphia: WB Saunders; 1996:678, with permission.)

The morphologic right atrial appendage is a broad-based triangular structure, and the left atrial appendage is a narrow-based fingerlike structure. Either type of isomerism may be associated with other anomalies, right isomerism with total anomalous pulmonary venous return, a large or common atrium, a common AV valve, a large VSD or single ventricle, TGA or double-outlet right ventricle, and pulmonary stenosis or atresia, whereas left isomerism often has associated partial anomalous pulmonary venous return, ASD, VSD, normal ventriculoarterial connection or double-outlet right ventricle or mitral stenosis, subaortic stenosis, aortic stenosis, and coarctation. All of these associated anomalies can be detected by using transaxial and coronal SE MRI. The severity of obstructive lesions can be assessed by using phase-contrast MRI techniques.

Aortic Anomalies

As a result of persistent and continued patency or disappearance of segments of the aortic arches, anomalies such as patent ductus arteriosus, double aortic arch, right aortic arch, anomalous right subclavian artery, interrupted aortic arch, or absent left pulmonary artery can be explained. A left aortic arch with an aberrant right subclavian artery is the most common aortic arch anomaly, with 0.5% prevalence in the population (59). The right subclavian artery and the distal right arch are incorporated into the descending aorta. The right ductus arteriosus is obliterated. The right subclavian artery can arise directly from the aorta or from an aortic diverticulum of Kommerell, that is, the persistent segment of the distal right dorsal aortic arch (Fig. 11). The aberrant right subclavian artery is best studied by SE transaxial and coronal imaging (42,60,61), and this feature is often found as an isolated anomaly. However, there is an increased inci-



Figure 11. Coronal SE MR image of an aneurysm of Kommerell situated at the junction of the left-subclavian artery and the aortic arch. The aneurysm was associated with partial rupture and subsequently underwent surgical repair.

dence with tetralogy of Fallot and coarctation. If the aberrant artery arises distal to the coarctation, it serves as a major collateral vessel, and rib notching is unilaterally confined to the left hemithorax.

A mirror-image right aortic arch is almost always (>95%) seen in conjunction with cyanotic CHD (56); 25% of patients with tetralogy of Fallot, 35–50% of patients with persistent truncus arteriosus, and 10% of patients with TGA have mirror-image right aortic arches. Tetralogy of Fallot is much more common (10–12% of CHD) than persistent truncus arteriosus (1.5–2.0%), and mirror-image right aortic arch is frequently associated with tetralogy of Fallot (Fig. 9). The more common form of a right aortic arch is the right arch with an aberrant left subclavian artery, which occurs in approximately 0.1% of the population (56). The frequency of CHD associated with this aortic anomaly is about 5%. Depiction of the pathoanatomy of the aberrant subclavian artery is best done using transaxial and coronal SE MRI (45,57,58). Transaxial imaging just below the arch nicely demonstrates the origin of the aberrant vessel and its course posterior to the esophagus. Using the same imaging plane, cine MRI can evaluate the amount of constriction the ring exerts on the esophagus and trachea during the cardiac cycle. Coronal SE MRI demonstrates the aorta to either the right or left of the spine.

Two types of double aortic arch are known and may be completely evaluated with MRI (45,59–61). When the diagnosis is suspected on the basis of clinical presentation or from plain chest radiography, MRI should be used as the primary noninvasive imaging modality. The caliber of both arches and the superior location of the right arch are best shown with coronal SE MRI. The encirclement of the trachea and esophagus by the classic inverted U appearance of the double aortic arch is best shown using transaxial SE MRI and cine-MRI.

Coarctation

Coarctation is a common anomaly resulting from a localized deformity of the aortic media that causes an eccentric infolding of the posterolateral wall of the proximal descending aorta (62). Rarely, the coarctation can occur proximal to the left subclavian artery or proximal to the ductus arteriosus (preductal, infantile form with hypoplasia of the aortic isthmus) (59). With either form of coarctation, there is usually dilatation of the aorta just distal to the coarctation site. This is due to the eccentric high-velocity blood jet caused by the coarctation. With high-grade stenosis, collateral vessels develop to reestablish flow to the descending aorta but cause a trans-

stenotic gradient (Fig. 3). MRI, with its large FOV, multiplanar format, and dynamic imaging, including velocity measurement, has emerged as the imaging modality of choice in the evaluation and follow-up of coarctation (63–66). Transaxial SE imaging can demonstrate the small caliber of the descending aorta but does not usually demonstrate the membrane or its relationship to the branch arteries. SE MRI performed in the LAO plane through the middle of the ascending and descending aorta “unfolds” the aorta and the site of coarctation, any hypoplasia of the aortic isthmus, and postcoarctation dilatation of the descending aorta. Especially MRA after injection of gadolinium-DTPA depicts the luminogram of the hypoplastic arch and the isthmus and nicely demonstrates enlarged intercostal collateral arteries when they are present (Fig. 12). Cine and phase-contrast MRI performed in LAO allows semiquantitative assessment of coarctation severity. Phase-contrast MRI performed distal to the coarctation site and perpendicular to the blood jet or in the LAO plane measuring velocity in three orthogonal planes is used to measure blood velocity distal to the coarctation (Fig. 3B). This can be used to calculate a pressure gradient using the modified Bernoulli equation with a pressure gradient of four times the peak velocity squared. Phase mapping can also be used to identify reversal of flow in the intercostal arteries or an aberrant right subclavian artery, documenting collateral flow to the descending aorta. Short-axis cine MRI is used to detect left ventricular hypertrophy and evaluate ventricular function. Similarly, SE transaxial MRI is used to scan the heart for any associated VSD, another commonly associated anomaly.

POSTSURGICAL EVALUATION AND FLOW DYNAMICS

All aforementioned MR techniques are by nature well suited for postsurgical assessment, both as a quality control measure and for follow-up management of any complex surgical procedure. However, patients with intraoperative placement of ferromagnetic vascular clips and coils constitute a contraindication for MRI at high field strength, whereas metal bone clips and wires may just cause local artifact.

Postoperative Tetralogy of Fallot

Despite improved surgical methods, pulmonary stenosis and pulmonary regurgitation are common postoperative sequelae after repair of tetralogy of Fallot and have been associated with enhanced risk of sudden death

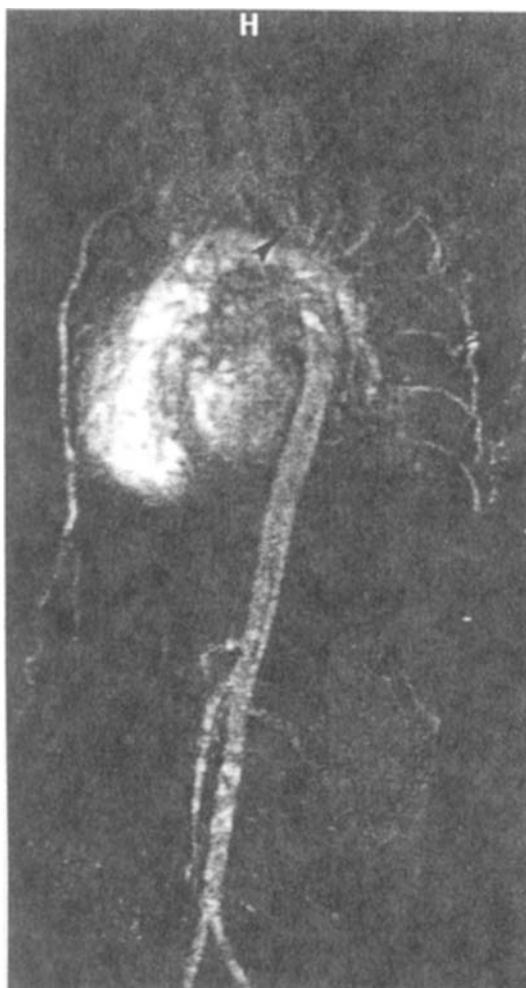


Figure 12. 3-D MRA after bolus injection of gadolinium-DTPA in a patient with coarctation; the MRA is ideal to demonstrate the development of collaterals via the intercostal and mammary arteries as evidence of a severe aortic narrowing. Note also the small aortic arch dimension (arrow).

(67,68). SE and GRE MRI are effective for the postsurgical evaluation of the anatomic and functional status. Pulmonary regurgitation is commonly found, especially when a transannular patch has been used for abolition of right ventricular outflow tract obstruction. The evaluation of the clinical significance of pulmonary regurgitation after Fallot repair has been facilitated with MRI. Phase-contrast MRI has been shown to be an accurate method for noninvasive volumetric quantification of pulmonary regurgitation after surgical correction of tetralogy of Fallot (69). In addition, multislice GRE MRI is an accurate method for performing measurements of right ventricular

volumes, without the limitations inherent to the complex geometry of the right ventricle (70,71). The consequences of pulmonary regurgitation on right ventricular function in patients who have undergone Fallot repair can be comprehensively evaluated with combined use of phase-contrast MRI and GRE MRI. Furthermore, the measurement of left and right ventricular stroke volumes based on the tomographic method can be used as an internal reference to validate the direct measurement of pulmonary flow; pulmonary regurgitation volumes closely agreed with the difference between the corresponding right and left ventricular stroke volumes as measured tomographically by GRE MRI (69). The comparison between MR velocity mapping results and regurgitation as judged from Doppler echocardiography showed that reliable assessment of the severity of pulmonary regurgitation is problematic with Doppler echocardiography and may be measured more reliably with phase-contrast MRI. Thus, phase-contrast MRI appears to be ideally suited for monitoring pulmonary regurgitation and right ventricular function after repair of tetralogy by Fallot (69).

Evaluation of Pulmonary Flow Dynamics

Various complex operations have been advised for cyanotic patients with CHD to enhance pulmonary blood flow. SE MRI is ideal to visualize the anatomy of pulmonary circulation and surgical procedures aimed at the improvement of pulmonary blood flow (2); the technique is superior to echocardiography to delineate the confluence of the pulmonary arteries in patients with pulmonary atresia (48,53). Also, MRI has an advantage over angiography in small children and pulmonary hypertension, both unlikely to tolerate application of contrast dye well. Both size and patency of systemic-to-pulmonary artery shunts can be assessed with great detail by SE MRI or flow-sensitive sequences without any need for contrast angiography (Fig. 2) (53).

Shunts and Conduits

Accurate diagnosis of obstruction in extracardiac conduits is well performed with the use of MRI techniques (72). A variety of conduits exists for improvement of the pulmonary flow in patients with cyanotic heart disease.

In *Rastelli's operation*, a conduit establishes or improves blood flow from the right ventricle to the pulmonary vasculature and may be visualized by gadolinium-enhanced MRA (Fig. 5). When a stenosis in the conduit is defined with SE MRI, MR velocity mapping can be used to calculate the pressure gradient across an ob-

structed conduit by applying a modified Bernoulli equation (similar to Doppler ultrasound) (72,73). The *Fontan procedure* and its related variations are designed to direct systemic venous return to the lungs (74,75). Modifications vary from direct atriopulmonary connection between the right atrium and the pulmonary artery to an AV connection between the right atrium and the right ventricle, incorporating the pumping capability of the right ventricle into the pulmonary circulation (Fig. 2). MR velocity mapping has proven suitable for the study of pulmonary flow patterns after Fontan surgery with both atriopulmonary and AV shunts (76). Monophasic systolic pulmonary flow curves are often seen in patients with AV Fontan connections, indicating right ventricular-dependent pulmonary blood flow. Usually, however, the pumping capabilities of the right ventricle are more or less a passive conduit in the Fontan circulation. Thus, MR velocity mapping provides reliable measurements of volume and velocity of pulmonary flow in various modifications of Fontan procedures and may objectively assess the success of Fontan procedure and flow distribution to both lungs or may be preferential to the left lung (76,77).

Pulmonary Hypertension

Assessment of pulmonary flow by MR velocity mapping gives insight into the severity of arterial pulmonary hypertension (78). Decreased pulmonary blood and lower peak systolic pulmonary flow velocities may be observed with severe pulmonary hypertension (79). Furthermore, the signal intensity in the right pulmonary artery on SE MR images appears to have a direct linear relationship with pulmonary vascular resistance in patients with congenital cardiovascular shunt lesions. Moreover, MR evaluation is by nature not harmful, contrary to the application of contrast dye in pulmonary hypertension.

Evaluation after Senning or Mustard Repair

Mustard or Senning operations redirect the pulmonary venous return to the anatomic right ventricle in patients with TGA and subject the right ventricle to the loading conditions of a systemic ventricle. Because the right ventricle is not ideally suited for systemic performance, right ventricular failure may develop in these patients. MRI may be of value in demonstrating baffle obstruction and in monitoring right ventricular systolic function in this category of patients. The ability of MRI to measure right ventricular diastolic function further qualifies this technique as a valuable tool for postsurgical evaluation before

systolic dysfunction is evident after Mustard and Senning operations (80). Abnormal tricuspid flow patterns by Doppler echocardiography after Mustard or Senning repair may result from reduced compliance and impaired relaxation of the hypertrophied right ventricle. MR velocity mapping of tricuspid flow in patients after Mustard or Senning repair has shown that abnormal tricuspid flow profiles can be demonstrated with MR velocity mapping. In patients after Mustard or Senning repair, the time to peak filling rate and normalized peak filling rate are usually higher than in normal children at similar age, body surface area, and heart rate.

SUMMARY AND FUTURE PERSPECTIVES

Currently, MR techniques provide useful information that is not readily available from other noninvasive modalities such as echocardiography, radionuclide imaging techniques, and computed tomography. The superb resolution, the inherent contrast, the 3-D nature, and its morphologic and functional imaging capabilities justify the application of MRI in all patients with CHD. The development of one single comprehensive procedure for studying cardiovascular anatomy, function, flow, coronary angiography, myocardial perfusion, and cardiac metabolism will be a major challenge both for diagnostic and for follow-up imaging. Although the number of MR machines is rapidly increasing, very fast real-time MRI is possible only in few centers with specially designed and dedicated magnets. Technologic improvement in hardware (rapid switching of magnetic field gradients) and software is emerging for fast-image acquisition on commercially available hospital-based magnets (81). MR contrast agents such as blood pool agents for CHD and compounds specifically absorbed by ischemic myocardial tissue are currently entering the clinical arena and offer new applications for MRI and MRA. With the advances in technology, replacement of a diagnostic test battery by just one primary MR procedure is just a question of conception and most likely beneficial for patient care and healthcare economics.

ACKNOWLEDGMENT

We are indebted to Profs. M. Davidoff and A. Holstein at the Department of Anatomy in the University Hospital Eppendorf for their review of the cardiac embryology. We also thank Mrs. J. Hoffmann and D. Oestreich for the expert secretarial and photographic support.

REFERENCES

1. Canter CE, Guitierrez FR, Mirowitz, et al. Evaluation of pulmonary morphology in cyanotic congenital heart disease by magnetic resonance imaging. *Am Heart J*, 1989; 118:347-354.
2. Formanek AG, Witcofski RL, D'Souza VJ, et al. MR imaging of the central pulmonary arterial tree in conotruncal malformation. *AJR Am J Roentgenol*, 1986; 147:1127.
3. Link KM and Lesko NM. Magnetic resonance imaging in the evaluation of congenital heart disease. *Magn Reson Imaging*, 1991; 7:173-190.
4. Szolar DH, Sakuma H and Higgins CB. Cardiovascular applications of magnetic resonance flow and velocity measurements. *JMRI*, 1996; 1:78-89.
5. Fletcher BD, Jacobstein MD, Nelson AD, et al. Gated magnetic resonance imaging of congenital cardiac malformations. *Radiology*, 1984; 150:137-144.
6. Hasse A, Frahm J, Matthaei D, et al. FLASH imaging: Rapid NMR imaging using low flip angle pulses. *J Magn Reson*, 1986; 67:258-264.
7. Dinsmore RE, Wismer GL, Levine RA, et al. Magnetic resonance imaging of the heart: Positioning and gradient angle selection for optimal imaging planes. *AJR Am J Roentgenol*, 1984; 143:1135-1141.
8. Bradley WG and Waluch V. Blood flow: Magnetic resonance imaging. *Radiology*, 1985; 154:443-449.
9. Hirsch R, Kilner PJ, Connelly MS, et al. Diagnosis in adolescents and adults with congenital heart disease: Prospective assessment of individual and combined roles of magnetic resonance imaging and transesophageal echocardiography. *Circulation*, 1994; 90:2937-2951.
10. Doornbos J and deRoos A. Imaging strategy in cardiac magnetic resonance imaging. In: van der Wall EE and deRoos A, eds. *Magnetic Resonance Imaging in Coronary Artery Disease*. Dordrecht: Kluwer, 1991.
11. Chung KJ, Simpson IA, Newman R, et al. Cine magnetic resonance imaging for evaluation of congenital heart disease: Role in pediatric cardiology compared with echocardiography and angiography. *J Pediatr*, 1988; 113:1028-1036.
12. Chung KJ, Simpson IA, Glass RF, et al. Cine magnetic resonance imaging after surgical repair in patients with transposition of the great arteries. *Circulation*, 1988; 77:104-109.
13. Van Ruge FP, van der Wall EE, van Dijkman PRM, et al. Usefulness of ultrafast magnetic resonance imaging in healed myocardial infarction. *Am J Cardiol*, 1992; 70:1233-1240.
14. Davis CP, McKinnon GC, Debatin JF, et al. Normal heart: Evaluation with echo-planar MR imaging. *Radiology*, 1994; 191:691-697.
15. Manning WJ, Atkinson DJ, Grossman W, et al. First-pass nuclear magnetic resonance imaging studies using gadolinium-DTPA in patients with coronary artery disease. *J Am Coll Cardiol*, 1991; 18:959-966.
16. Guifoye DN, Gibbs P, Ordidge RJ, et al. Real-time flow measurements using echo-planar imaging. *Magn Reson Med*, 1991; 18:1-9.
17. Wendland MF, Saeed M, Masui T, et al. Echo-planar MR imaging of normal and ischemic myocardium with gadodiamide injection. *Radiology*, 1993; 186:535-540.
18. Seelos KC, von Smekal A, Vahlensieck M, et al. Cardiac abnormalities: Assessment with T2-weighted turbo spin-echo MR imaging with electrocardiogram gating at 0.5 T. *Radiology*, 1993; 189: 517-522.
19. Nienaber CN, von Kodolitsch Y, Petersen B, Loose R, Helmchen U, Haverich A and Spielmann RP. Intramural hemorrhage of the thoracic aorta: Diagnostic and therapeutic implications. *Circulation*, 1995; 92:1465-1472.
20. Prince MR, Narasimham DL, Jacoby WT, Williams DM, et al. Three-dimensional gadolinium-enhanced MR angiography of the thoracic aorta. *AJR Am J Roentgenol*, 1996; 166:1387-1397.
21. Bradley WG. Flow phenomena in MR imaging. *AJR Am J Roentgenol*, 1988; 150:983-989.
22. Mohiaddin RH and Longmore DB. Functional aspects of cardiovascular nuclear magnetic resonance imaging: Techniques and application. *Circulation*, 1993; 88:264-269.
23. Rebergen SA, van der Wall EE, Doornbos J, et al. Magnetic resonance measurement of velocity and flow: Technique, validation, and clinical applications. *Am Heart J*, 1993; 126:1439-1445.
24. Firmin DN, Nayler GL, Klipstein RH, et al. In vivo validation of MR velocity imaging. *J Comput Assist Tomogr*, 1987; 11:751-758.
25. Mohiaddin RH, Wann SL, Underwood R, et al. Vena caval flow: Assessment with cine MR velocity mapping. *Radiology*, 1990; 177:537-543.
26. Mohiaddin RH, Amanuma M, Kilner PJ, et al. MR phase-shift velocity mapping of mitral and pulmonary venous flow. *J Comput Assist Tomogr*, 1991; 15:237-242.
27. Mohiaddin RH, Paz R, Theodoropoulos S, et al. Magnetic resonance characterization of pulmonary arterial blood flow after single lung transplantation. *J Thorac Cardiovasc Surg*, 1991; 101:1016-1020.
- 27a. Brenner LD, Caputo GR, Mostbeck G, et al. Quantification of left to right atrial shunts with velocity-encoded cine nuclear magnetic resonance imaging. *J Am Coll Cardiol*, 1992; 20:1246-1250.
28. Prince MR, Narasimham DL, Jacoby WT, Williams DM, et al. Three-dimensional gadolinium-enhanced MR angiography of the thoracic aorta. *AJR Am J Roentgenol*, 1996; 166:1387-1397.
29. Krinsky GA, Rofsky NM, DeCorato DR, Weinreb JC, et al. Thoracic aorta: Comparison of gadolinium-enhanced three-dimensional MR angiography with conventional MR imaging. *Radiology*, 1997; 202:183-193.
30. Van Praagh R. The segmental approach to diagnosis in congenital heart disease. *Birth Defects*, 1972; 8:4-12.
31. Eidemiler LR and Keane JM. Development of the heart.

- In: Pearson AA, ed. *The Development of the Cardiovascular System*. Portland, OR: University of Oregon Medical School Printing Department; 1968:42–65.
32. Moore KL. *The Circulatory System: The Cardiovascular and Lymphatic Systems*. 2nd ed. Philadelphia: WB Saunders; 1977:24–50.
 33. Netter FH. Embryology. In: Yonkman FF, ed. *The CIBA Collection of Medical Illustrations*. West Caldwell, NJ: CIBA; 1978:112–128.
 34. Landing BH, Lawrence TK, Payne VC, Wells TR. Bronchial anatomy in syndromes with abnormal visceral situs, abnormal spleen and congenital heart disease. *Am J Cardiol*, 1971; 28:456–460.
 35. Partridge JB, Scott O, Deverall PB and Macartney FJ. Visualization and measurement of the main bronchi by tomography as an objective indicator of thoracic situs in congenital heart disease. *Circulation*, 1975; 51:188–195.
 36. Van Mierop LHS, Eisen S and Schiebler GL. The radiographic appearance of the tracheobronchial tree as an indicator of visceral situs. *Am J Cardiol*, 1970; 26:432–440.
 37. Masui T, Seelos KC, Kersting-Sommerhoff BA, et al. Abnormalities of the pulmonary veins: Evaluation with MR imaging and comparison with cardiac angiography and echocardiography. *Radiology*, 1991; 181:645–651.
 38. Huggon IC, Baker EJ, Maisey MN, et al. Magnetic resonance imaging of hearts with atrioventricular valve atresia or double inlet ventricle. *Br Heart J*, 1992; 68:313–319.
 39. Kersting-Sommerhoff BA, Diethelm L, Stanger P, et al. Evaluation of complex congenital ventricular anomalies with magnetic resonance imaging. *Am Heart J*, 1990; 120:133–140.
 40. Parsons JM, Baker EJ, Anderson RH, et al. Double-outlet right ventricle: Morphologic demonstration using nuclear magnetic resonance imaging. *J Am Coll Cardiol*, 1991; 18:168–175.
 41. Rebergen SA, Guit GL and de Roos A. Double outlet left ventricle: Assessment with magnetic resonance imaging. *Br Heart J*, 1991; 66:381–390.
 42. Perloff JK. *The Clinical Recognition of Congenital Heart Disease*. 4th ed. Philadelphia: WB Saunders; 1994:69.
 43. Van Praagh R, Ongley PA and Swan HJC. Anatomic types of single or common ventricles in man: morphologic and geometric aspects of 60 necropsied cases. *Am J Cardiol*, 1964; 13:367–386.
 44. Guit, GL, Bluemm R, Rohmer J, et al. Levotransposition of the aorta: Identification of segmental cardiac anatomy using MR imaging. *Radiology*, 1986; 161:673–679.
 45. Kersting-Sommerhoff BA, Sechtem UP, Fisher MR and Higgins CB. MR imaging of congenital anomalies of the aortic arch. *AJR Am J Roentgenol*, 1987; 149:9–15.
 46. Lowe GM, Donaldson JS and Backer CL. Vascular rings: 10 year review of imaging. *Radiographics*, 1991; 11: 637–641.
 47. Kersting-Sommerhoff BA, Diethelm L, Teitel DF, et al. Magnetic resonance imaging of congenital heart disease: Sensitivity and specificity using receiver operating characteristic curve analysis. *Am Heart J*, 1989; 118:155–161.
 48. Rees RSO, Somerville J, Underwood SE, et al. Magnetic resonance imaging of the pulmonary arteries and their systemic connections in pulmonary atresia: Comparison with angiographic and surgical findings. *Br Heart J*, 1987; 58:621–626.
 49. Bornemeier RA, Weinberg PM, Fogel MA. Angiographic, echocardiographic, and three-dimensional magnetic resonance imaging of extracardiac conduits in congenital heart disease. *Am J Cardiol*, 1996; 78:713–717.
 50. Baker EJ, Ayton V, Smith MA, et al. Magnetic resonance imaging at a high field strength of ventricular septal defects in infants. *Br Heart J*, 1989; 62:305–309.
 51. Didier D and Higgins CB. Identification and localization of ventricular septal defect by gated magnetic resonance imaging. *Am J Cardiol*, 1986; 57:1363–1371.
 52. Diethelm L, Dery R, Lopton MJ, et al. Atrial-level shunts: sensitivity and specificity of MR in diagnosis. *Radiology*, 1987; 152:181–188.
 53. Kersting-Sommerhoff BA, Sechtem UP and Higgins CB. Evaluation of pulmonary blood supply by nuclear magnetic resonance in patients with pulmonary atresia. *J Am Coll Cardiol*, 1988; 11:166–172.
 54. Sechtem UP, Pflugfelder P, Cassidy MC, et al. Ventricular septal defect: Visualization of shunt flow and determination of shunt size by cine MR imaging. *AJR Am J Roentgenol*, 1987; 149:689–694.
 55. Fogel MA and Rychik J. Right ventricular function in congenital heart disease: Pressure and volume overload lesions. *Prog Cardiovasc Dis*, 1998; 40:343–356.
 56. Van Praagh R. The importance of segmental situs in the diagnosis of congenital heart disease. *Semin Roentgenol*, 1985; 20:254–261.
 57. Stanger P, Rudolph AM and Edwards JE. Cardiac malpositions: an overview based on study of sixty-five necropsy specimens. *Circulation*, 1977; 56:159–172.
 58. Park ET, Han MC and Kim C. MR imaging of congenitally corrected transposition of the great vessels in adults. *AJR Am J Roentgenol*, 1989; 143:491–497.
 59. Stewart JR, Kincaid OW and Edwards JE. *An Atlas of Vascular Rings and Related Malformations of the Aortic Arch System*. Springfield, IL: Charles C Thomas; 1964.
 60. Link KM. Great vessels. In: Stark DD, Bradley WG Jr, eds. *Magnetic Resonance Imaging*. 2nd ed. St. Louis: Mosby-Year Book; 1991:1490–1530.
 61. Bisset GS III, Strife JL, Kirks DR and Bailey WW. Vascular rings: MR imaging. *AJR Am J Roentgenol*, 1987; 149:251–258.
 62. Freedom RM, Culham JAG and Moes CAF. *Angiocardiology of Congenital Heart Disease*. New York: Macmillan; 1984.

63. Connelly MS, Webb GD, Somerville J, Warnes CA, Perloff JK, et al. Canadian consensus conference on adult congenital heart disease 1996. *Can J Cardiol*, 1998; 14: 395-452.
64. Bank ER, Aisen AM, Rocchini AP, et al. Coarctation of the aorta in children undergoing angioplasty: Pretreatment and posttreatment MR imaging. *Radiology*, 1987; 162:235-240.
65. Julsrud PR, Breen JF, Fehlee JP, Warnes CA, et al. Coarctation of the aorta: Collateral flow assessment with phase-contrast MR angiography. *AJR Am J Roentgenol*, 1997; 169:1735-1742.
66. Oshinski JN, Parks WJ, Markou CP, Bergman HL, et al. Improved measurement of pressure gradients in aortic coarctation by magnetic resonance imaging. *J Am Coll Cardiol*, 1996; 28:1818-1826.
67. Helbing WA, Niezen RA, Le Cessie S, van der Geest RJ, et al. Right ventricular diastolic function in children with pulmonary regurgitation after repair of tetralogy of Fallot: Volumetric evaluation by magnetic resonance velocity mapping. *J Am Coll Cardiol*, 1996; 28:1827-1835.
68. Marie PY, Marcon F, Brunotte F, et al. Right ventricular overload and induced sustained ventricular tachycardia in operatively "repaired" tetralogy of Fallot. *Am J Cardiol*, 1992; 69:785-791.
69. Rebergen SA, Chin JG, Ottenkamp J, et al. Pulmonary regurgitation in the late postoperative follow-up of tetralogy of Fallot: Volumetric quantification by nuclear magnetic resonance velocity mapping. *Circulation*, 1993; 88: 2257-2266.
70. Niwa K, Uchishiba M, Aotsuka H, Tobita K, et al. Measurement of ventricular volumes by cine magnetic resonance imaging in complex congenital heart disease with morphologically abnormal ventricles. *Am Heart J*, 1996; 131:567-575.
71. Mogelvang J, Stubgaard M, Thomsen C, et al. Evaluation of right ventricular volumes measured by magnetic resonance imaging. *Eur Heart J*, 1988; 9:529-536.
72. Martinez JE, Mohiaddin RH, Kilner PJ, et al. Obstruction in extracardiac ventriculopulmonary conduits: Value of nuclear magnetic resonance imaging with velocity mapping and Doppler echocardiography. *J Am Coll Cardiol*, 1992; 20:338-343.
73. Eichenberger AC, Jenni R, Von Schulthess GK. Aortic valve pressure gradients in patients with aortic valve stenosis: Quantification with velocity-encoded cine MR imaging. *AJR Am J Roentgenol*, 1993; 160:971-976.
74. Fontan F and Baudet E. Surgical repair of tricuspid atresia. *Thorax*, 1971; 26:240-248.
75. DeLeon SY, Ilbawi MN, Idriss FS, et al. Fontan type operation for complex lesions. *J Thorac Cardiovasc Surg*, 1986; 92:1029-1036.
76. Rebergen SA, Ottenkamp J, Doornbos J, et al. Postoperative pulmonary flow dynamics after Fontan surgery: Assessment with nuclear magnetic resonance velocity mapping. *J Am Coll Cardiol*, 1993; 21:123-131.
77. Caputo GR, Kondo C, Masui T, et al. Right and left lung perfusion: In vitro and in vivo validation with oblique-angle velocity-encoded cine MR imaging. *Radiology*, 1991; 180:693-699.
78. Bogren HG, Klipstein RH, Mohiaddin RH, et al. Pulmonary artery distensibility and blood flow patterns: A magnetic resonance study of normal subjects and of patients with pulmonary arterial hypertension. *Am Heart J*, 1989; 118:990-995.
79. Kondo C, Caputo GR, Masui T, et al. Pulmonary hypertension: Pulmonary flow quantification and flow profile analysis with velocity-encoded cine MR imaging. *Radiology*, 1992; 183:751-758.
80. Rebergen SA, Helbing WA, van der Wall EE, et al. MR velocity mapping of tricuspid flow in healthy children and patients who have undergone Mustard or Senning repair. *Radiology*, 1995; 194:505-511.
81. Boxerman JL, Mosher TJ, McVeigh ER, Atalar E, Lima JAC and Bluemke DA. Advanced MR imaging techniques for evaluation of the heart and great vessels. *RadioGraphics*, 1998; 18:543-564.